Proceedings World Geothermal Congress 2026
Calgary, Canada, June 8 – 11, 2026

Analysis of entropy generation and productivity index using airlift system with different gas injectors to extract heat from geothermal brine

J. Gutierrez-Martinez[1]*, J. J. Pacheco- Ibarra[2], C. Rubio-Maya[3], A. Gutierrez-Martinez, S. R. Galvan-Gonzalez.

Faculty of Mechanical Engineering UMSNH*, Faculty of Mechanical Engineering UMSNH[2], Faculty of Mechanical Engineering UMSNH[3]

E-mail address for corresponding author only indicated by (*): jgutierrez@umich.mx

Keywords: Entropy generation, heat transfer, airlift system, injectors, productivity index, submergence ratios.

ABSTRACT

An analysis of entropy generation and the productivity index during heat extraction in geothermal brine is presented using a concentric airlift pumping system with nozzles of different total areas for gas injection and varying submergence ratios in a 1,344-meter-deep geothermal well. From the collected data, both the productivity index and the entropy generation are obtained through thermodynamic analysis. The results show that, during the geothermal brine extraction process, entropy generation decreases both with higher submergence ratios and with nozzles with larger gas injection areas at a constant flow rate. This increases the temperature of the extracted brine and the productivity index. It can be concluded that: by increasing the immersion ratios, as well as the total area for gas injection with the nozzles, the velocity of the geothermal brine in the riser pipe inside the well is increased, thereby reducing heat loss to the geothermal reservoir through heat transfer. Therefore, an increase in the temperature and flow variables extracted within the experimental range is observed.

1.INTRODUCTION

It is known that electricity can be generated from medium- and low-enthalpy geothermal resources using certain technologies (Arslan et al., 2010). Downhole pumps are required for geothermal brine extraction, especially in large-scale direct-use systems. The two most common types are straight-shaft pumps and submersible pumps. In conventional geothermal applications, straight-shaft pumps are preferred over submersible pumps for two main reasons: the lowest cost of the linear shaft pump, also because it has a proven track record of effectiveness (Lund et al., 2020); however, they are subject to technical and operational failures related to abrasion and corrosion, requiring periodic maintenance, resulting in downtime. On the other hand, submersible pumps are necessary for depths greater than 250 m (Lund and Toth, 2020), with the disadvantage that these pumps can usually only operate with low liquid enthalpy values and temperatures up to 120 °C (Ware et al., 2020). In the literature, the determination of geothermal energy production in abandoned oil wells has been simulated using computational models by injecting a secondary fluid, such as isobutane, which is heated to produce steam. These systems have been observed to achieve a maximum power output dependent on the bottomhole temperature and injection pressure (Davis et al., 2009). Another technique used in oil extraction is the pneumatic lift pump, or airlift (Hanafizadeh et al., 2011). This pneumatic pumping technique has also been used for geothermal brine extraction, as reported by (Baujard et al., 2017; and Fisch et al., 2015). Even though this pumping technique has been used for more than two centuries, it continues to be of interest in different areas of engineering such as hydrodynamics, fluid dynamics, oceanography, and geothermal energy. Some applications in which it has been used: Evaluating the effect of tube diameter on airlift pump performance, considering surface tension on bubble velocity and immersion ratio (Reinemann et al., 1990). Simulating airlift pumps using different correlations (Zens et al., 1993). Predicting the pressure gradient for slug flow and study the performance of airlift pumping system using variable parameters (de Cachard et al., 1996). Analyzing a three-phase airlift system using a pseudo-liquid composed of liquid and solid phase (Margaris et al., 1997). Simulating numerically an airlift pump for a deepwater well (Nenes, 1997). Studying the application of airlift pumping in absorption refrigeration cycles, where this pumping system was highly dependent on the immersion ratios (White et al., 1999). Understanding the performance improvement mechanism with a hydrodynamic investigation using a tapered lift tube (Kumar et al., 2003). Measuring the performance and transition regime of airlift pumping where superficial gas and liquid velocity of the surface were used as map coordinates (Samaras et al., 2005). Developing a novel numerical physics approach to simulate two-phase flow in an airlift pump riser (Hanafizadeh et al., 2010). Evaluating the logistics of offshore deployment and equipment durability in geoengineering under extremely complex hydrodynamic conditions (Pan et al., 2019). Upwelling ocean water (Fan et al., 2013). Evaluating the influence of different air entry modes and riser pipe diameters on airlift pump

performance, where results showed that pumping efficiency decreased with smaller gas injection areas at the nozzles, and different perforation distributions had no significant influence on liquid flow rate and pumping efficiency was not significant (Zuo et al., 2020). Developing a method selecting the optimal airlift pumping operating regime, which provides stability and efficiency of liquid transport, in addition to which it can be applied to determine the correlation between the total lifting efficiency and the required gas flow (Ligus et al., 2019). Evaluating the different constant and pulsating air injection modes, where the results show that the performance of airlift pumps depends on the air injector design and the dynamics of the injection method, where the best results are obtained with both axial and dual pulsating injection modes attributed to the decrease of the reverse flow of water in the riser (Ahmed et al., 2016). Studying the effect of liquid temperature on airlift performance, where a high efficiency value is obtained at a low gas flow value and a high immersion ratio and temperature (Ouelasti et al., 2017). Modeling an airlift pump, by calculating entropy generation and exegetical analysis, at different immersion ratios and flow regimes, where the results show that entropy generation is lower in the slug-type regime with a low injection rate of volumetric airflow (Hanafizadeh et al., 2011). Based on the literature review, no studies have considered the effect of pressurized fluid temperature in a geothermal well using submergence ratios for a non-adiabatic system, nor have nozzle design with varying total injection areas, and air injection mode used, to determine entropy generation and productivity index with the airlift pumping system. With mechanical pumping and airlift systems, the objective is to obtain the highest possible volumetric flow rates and surface temperatures. For this purpose, thermodynamic properties are evaluated based on pressure and temperature (Michaelides et al., 1981). Although a geothermal system can operate continuously throughout the year, there are those that present medium and low enthalpies and require the use of technologies that allow brine to be extracted to the surface at a low initial cost, easy to operate and maintain, and with little space requirements. This is where this work becomes relevant. Furthermore, there are also some non-vertical wells where operating mechanical pumping systems is technically difficult, where an airlift pumping system is a feasible alternative. Additionally, given the high demand for batteries to store excess energy produced, it is important to develop alternatives that strengthen energy storage, as a mechanical, chemical and thermal energy (Mital et al., 2022). Pressurized gas is a form of mechanical energy storage that can be used to operate an airlift pumping system.

2. PROJECT OVERVIEW

The experimental work is carried out in a geothermal well located at coordinates 19°53'54" north latitude and 100°49'50" west longitude, with a depth of 1344 m (meters), it is identified as Z-3, which is located about 20 km west of the Los Azufres geothermal field in the Araró geothermal field that is part of the Mexican Volcanic Belt (Central Part of Mexico). The airlift pumping system is installed inside the geothermal well and consists of a steel pipe for lifting the mixture, with a length and diameter of 140 and 0.1016 m respectively; and a steel pipe for injection with a diameter of 0.00254 m. The gas is introduced into the geothermal well concentrically at four different SR submergence ratios (0.80, 0.85, 0.90 and 0.91). The liquid level in the geothermal well is 3 m below the surface where the pipe is introduced to raise the l-g mixture. In addition, the mechanical condition of well Z-3 is shown in (Table 1).

Table 1. Mechanical condition of the geothermal well.

Well diameter (cm)	Pipe diameter (cm)	Depth (m)	Description
66.04	50.8	18.1	Well
44.45	33.973	363.6	Well
31.11	Without tube	1344	Well

2.1 Depths at which gas injection was carried out

The depth at which air is injected has been increased, i.e., 30, 42, 66, and 72 m depth in different tests to control the submergence ratio (SR) represented by eq. (2.1) consists of the ratio of lengths from the injection point (Ls) to the liquid level (Lg) in relation to the length from the injection point (Ls) to the surface (L) (Hanafizadeh et al., 2011).

$$SR = (Ls - Lg)/(L - Lg) \quad (2.1)$$

orrespond to the SR immersion ratios of 0.80, 0.85, 0.90, and 0.91, respectively. Four different injectors are used for each of these. A 60 hp screw compressor, a pressure regulator, and a variable area flowmeter are used for the compressed air supply. Compressed air is supplied at a constant volumetric flow rate of 87 lt/s through the steel pipe to the air injector at pressures ranging from 4.20 to 6.00 kg-f /cm^2 and at temperature of 40 °C. To calculate the inlet air density, instantaneous air pressure and temperature are recorded every 10 minutes for 4 hours for each test, and the instantaneous mass flow rate is then obtained. The injectors were screwed to the lower end of riser tube for all 4 immersions, introducing the air injections from the compressor.

2.2 Water composition, thermal and mechanical measurements.

The physical and chemical analysis of the brine indicates the following parameters: sodium chloride at 759 ppm, chlorides at 1064 ppm, sulfates at 56 ppm, boron at 174 ppm (mg/lt), magnesium at 14 ppm, calcium at 16 ppm, and potassium at 49 ppm. An electronic probe called K-10 was subsequently introduced into the Z-3 geothermal well, with an accuracy of ± 0.025% for pressure and ± 0.5 °C for temperature. It is observed that, according to the thermodynamic Clapeyron curve, the column within the well is in the subcooled liquid zone. From the surface to approximately 102 m, the temperature rises rapidly to 145 °C; this is followed by a further increase to 146 °C at a depth of 225 m. From 250 m there is a decrease of 4°C until 500 m, which is inferred to a permeable zone below 350 m (see Fig. 1).

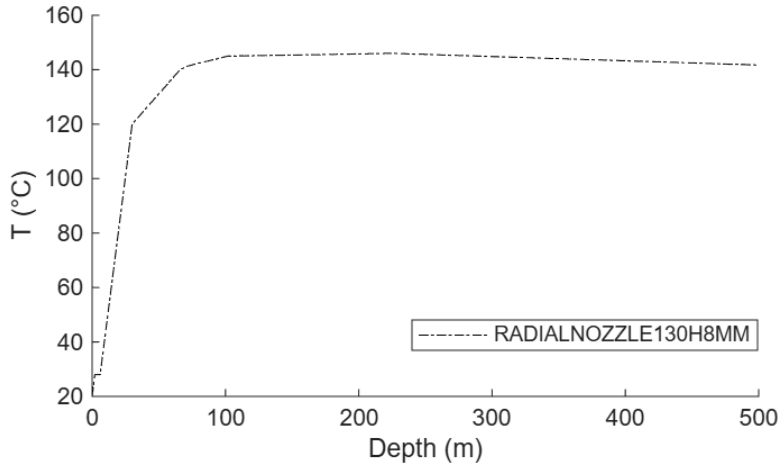


Fig. 1. Shows the thermodynamic profile of the geothermal well up to 500 meters deep; it can be seen that the temperature increases rapidly during the first 100 meters and then decreases very slightly.

2.3 Nozzles used for gas injection

Four different stainless-steel injectors with a diameter of 0.00254 meters (m), are used in the air injection tests; three of these, with a length of 0.20 (m), are used for radial injection identified as BR, followed by the number of perforations and their diameter. Another axial injector, identified as BA, is used with a length of 0.10 (m). The total gas injection areas are presented in (Table 2), which identifies the design of each injector.

Table 2. Identification of the total gas injection areas with the different injectors.

Nomenclature	Injection	# perforations	Diameter (mm)	Total injection area (m^2)
BR130P8MM	Radial	130	8	0.006534513
BR130P6MM	Radial	130	6	0.003675663
BR130P4MM	Radial	130	4	0.001633628
BA21P2.5MM	Axial	21	2.5	0.001030840

2.4 Thermodynamic analysis to determine entropy generation, Sgen.

The thermodynamic energy analysis is performed according to the work of (Hanafizadeh, et al. 2011) to determine the entropy generation during the brine extraction process under the aforementioned immersion ratios. It is considered a non-adiabatic brine extraction process. Therefore, heat transfer from the lift pipe to the reservoir and the injected gas is also considered, since the extraction process cool the liquid-gas mixture that rises to the surface and this has a considerable effect. The equations of the first and second laws of thermodynamics are used for each section of the airlift to study the effect of the different nozzles used in the airlift with different total gas injection areas.

2.5 Hydraulic test of the reservoir.

Hydraulic testing consists of well cleaning, brine production, measurements, flow stabilization, and obtaining the productivity index (flow rate/pressure drop). Well cleaning operations are performed on August (24 th-26th), 2019, with an average flow rate of 7.25 l/s (for 4 hours/day). Brine extraction began with an airlift without a gas injector, at a depth of 36 m. After this well cleaning phase, the production testing phase began without the use of a gas injector. However, due to the instability of flow rates, gas injectors are used for all tests, which facilitates the stabilization of the extracted flow rate and its subsequent measurement on August 27th at 10:00 hours and ending on September 4th, 2019. The extracted brine flow rates are presented in the range of (1.7 to 8.0) l/s, during four hours of testing with each injector and four submergence ratios. The four immersion ratios with each gas injector present different brine flow rates and temperatures. Data are collected under the same meteorological conditions on warm days, over 4-hour periods, with readings taken every 10 minutes. The flow rate is best stabilized with both injectors with larger flow areas and higher immersion ratios. Furthermore, well productivity under these conditions could be estimated at 2.33 l/s/kg-f/cm2. The maximum recorded brine temperature obtained is 108.5°C, with a flow rate of 8.0 l/s.

2.6 Thermodynamic properties, heat transfer and Sgen

To study the thermodynamic properties and heat transfer, a depth of seventy-two meters is used, corresponding to the greatest immersion at which air injection is performed. This is done in order to determine the thermodynamic properties and their relationship with entropy generation, using the second law of thermodynamics and heat transfer; for all the data obtained, the steady state is considered for the analysis; each test lasted four hours, and pressure, temperature, and flow readings are taken every ten minutes.

2.6.1 Thermodynamic properties

The thermodynamic properties of the brine are evaluated based on temperature, pressure, and sodium chloride molality (NaCl) (number of moles of solute/kg of solvent) (Michaelides et al., 1981). The NaCl concentration in the brine is found to be 759 milligrams/liter. Furthermore, the temperature at which the air mixes with the brine inside the well is evaluated, before ascending through the riser pipe as a two-phase mixture (liquid-gas) to the surface (Krasniqui et al., 2018).

2.6.2 Heat transfer and Sgen.

The heat transfer from the riser to the reservoir is then calculated using the first law of thermodynamics, and the entropy generation using the second law of thermodynamics. The heat transfer from the liquid-gas mixture (l-g) from inside the riser to the cooler reservoir brine as it approaches the surface occurs from the outer surface of the riser by natural convection (Qconv) and radiation (Qrad) and thermal conduction (Qcond) see equation (2.2), in agreement with other works (Najeeb et al., 2017).

$$Q_{out} = Q_{conv} + Q_{cond} + Q_{rad} \tag{2.2}$$

The temperatures reached by the brine upon reaching the liquid-gas mixing zone are calculated for the submergence ratios at 30, 42, 66 and 72 m, are 123.89, 131.68, 141.0 and 141.4 °C; the combined heat transfer coefficients (h_avg) are 11500 J/s.m2. K, respectively (Najeeb et al., 2017). The heat loss by thermal radiation between the outer surfaces of the pipe to the surrounding brine is calculated (Najeeb et al., 2017). The natural convection heat transfer Qconv can be calculated with Newton's cooling equation according to (Favre-Marient et al., 2009 and Bejan et al., 2013), see eq. (2.3).

$$Q_{conv} = h_{av}\, A_s (T_{sav} - T_{asurr}) \tag{2.3}$$

Where, Tasurr is the temperature of the reservoir surroundings, Tsav is the average temperature of the surface of the riser for the interval from (0 to L) in meters and L the length of the pipe (Suter et al., 1992). In addition, to evaluate the heat output from the riser to the reservoir, the data obtained with the energy balances are used, through equation (2.4), applying the first law of thermodynamics for each measurement, calculating a discharge temperature for the geothermal brine that is evaluated with the temperatures measured with the instruments (Hanafizadeh et al., 2011).

$$\dot{Q}_{VC} + \sum \dot{m}_i \left(h_i + \frac{V_i^2}{2} + gZ_i\right) = \frac{dE_{VC}}{dt} + \sum \dot{m}_e \left(h_e + \frac{V_e^2}{2} + gZ_e\right) + \dot{W}_{VC} \quad (2.4)$$

There is no work transfer across the boundaries of the control volume, and the process is considered to be steady. Air is represented by (a), brine by (b), the inlet to the control volume by (i), and the outlet of the system by (e). The air and brine at the outlet are considered to be in thermal equilibrium. Also, according to the law of conservation of matter, the masses of air and brine entering the airlift pump correspond to those exiting and are expressed in the equation. Next, the heat transferred from the mixture (l-g) in the riser pipe to the reservoir brine, which is colder as we approach the surface, is expressed in Eq. (2.5).

$$Q_{K1} = q_{VC} m_b \quad (2.5)$$

Meanwhile, the heat transfer from the rising tube with the l-g mixture to the air entering through the injection pipe to the mixing zone, see eq. (2.6) (Beasley et al., 2009).

$$Q_a = m_a C_{pa} (T_2 - T_1) \quad (2.6)$$

The equation (2.7) represents the heat transferred from the airlift to the reservoir brine which is colder, considering that the heat transferred to the injected gas remains in the mixture (l-g).

$$Q_{br1} = Q_k - Q_a \quad (2.7)$$

Subsequently, to calculate the temperature at which the air reaches the mixing zone and considering that this airlift pump has two concentric tubes of different diameters, of which the inner tube (smaller diameter) through which the air is injected and the outer tube where the mixture l-g is raised, so in this process there is a countercurrent heat exchange (Bejan et al., 2013). The outlet temperature of the cold air flow t_f is calculated with eq. (2.8) based on the length L of the pipe and the countercurrent heat exchange surface A and the temperature gradient.

$$t_f = \left(t_{f2} - t_{f1}\right).e^{-a_n.k.A_0}/(1 - e^{-a_n.k.A_0}) + \left(t_{f1} - t_{f2}\right)e^{-a_n.k.A}/(1 - e^{-a_n.k.A_0}) \quad (2.8)$$

Where, the subscripts f and n represent the cold and hot fluids, respectively, Cn and Cf are the specific heat rates, tf_1, tn_1 are the inlet temperatures, tf_2, tn_2 are the outlet temperatures, k is the overall heat transfer coefficient that is considered to be 40 (Watt/m^2. K) for gases in forced convection (Favre-Marient et al., 2009). Next, the heat transfer is calculated with the temperature at which the gas reached the l-g mixing point and with the temperature at which the brine is found when injecting the gas for each of the immersions, at the time of the l-g phase mixing. Subsequently, the second law of thermodynamics is used for the control volume, and the energy balance is presented in equation (2.9)

$$\frac{dSvc}{dt} + \sum \dot{m}_s \, S_s - \sum \dot{m}_e \, S_e = \int_0^t (\dot{Q}_{VC}/T)\, dt + S_{gen} \quad (2.9)$$

Considering the steady state as in the study by Hanafizadeh et al. (2011) for the riser tube of the airlift system. The specific heats at constant volume and pressure are identical for incompressible substances (Cengel et al., 2011). Air presents ideal gas characteristics under the principle of corresponding states, with constant specific heat, since T-Reduced > 2 and P-Reduced <<1. Then, the entropy generation is obtained in equation (2.10) (Cengel et al., 2011).

$$\dot{m}_a(Cp_{a,s}\, In\, (T_{a,s}/T_{a,e}) - R\, In(P_{a,s}/P_{a,e})) + \dot{m}_b C_b\, In(T_{b,s}/T_{b,e}) - \sum \dot{Q}_K / T_k = S_{gen} \quad (2.10)$$

Finally, the heat extracted from the geothermal brine is also calculated with equation (2.1

$$Q_{bextraido} = m_b C_b (T_b - T_{amb}) \quad (2.11)$$

2.7 Results

The data collected show the best results with the injector with the largest passage area (0.006534512 m^2) identified as BR130P8MM; compared to the other three injectors. The increase in flow is 14 % (6.9 to 8) l/s; while the increase in temperature obtained is 6.5 °C (102 to 108.5) °C. For this reason, the graphs obtained with the injector with the largest area are presented. The temperature (°C) of the extracted geothermal brine and the extracted liquid flow rate (l/s); are related in (Fig. 2). It is observed that for greater immersions the liquid temperature increases 40.5 °C (from 78 to 108.5) °C; while the flow rate also increases (from 1.7 to 8) l/s; so that increasing the immersion ratio from 0.80 to 0.91 represents a greater use of the geothermal resource.

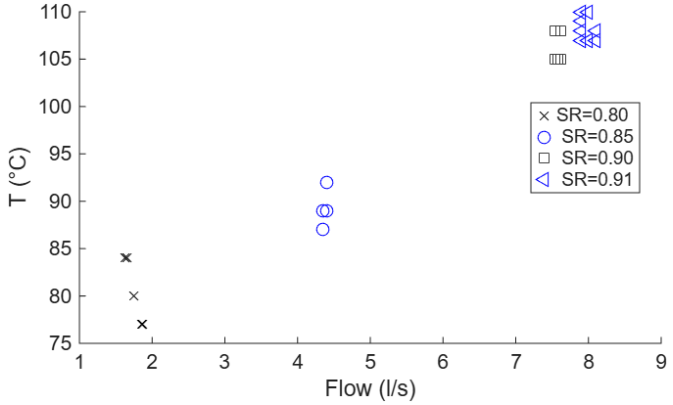


Fig. 2) Shows the relationship between T (°C) and flow rate (l/s); it can be seen that both variables increase with higher submergence ratios as the rate of rise of the l-g mixture increases.

The temperature (°C) of the extracted geothermal brine and Sgen (KW/K) are related in (Fig. 3); it is observed that for greater submergence ratios the liquid temperature increases considerably 40.5 °C (78 to 108.5) °C; while the average Sgen decreases 13 % (from 0.342 to 0.296) KW/K, as the immersion increases, which represents a greater use of the flow energy for the greater immersions.

The productivity index (l/s/kg. f/cm2) and Sgen (KW/K); are related in (Fig. 4). Where it can be observed that for greater submergence ratios (from 0.80 to 0.91) the productivity index increases significantly; that is, 1.5 (l/s/kg. f/cm2), which adjusts with the results presented by (Baujard et al., 2017 and Fisch et al., 2015). While the average Sgen decreases (from 0.342 to 0.296) KW/K, when the immersion increases; which represents a greater use of the flow energy for the greater immersions.

The relationship between pressure drop ΔP (kg f/cm^2) and Sgen (kW/K) is shown in (Fig. 5). It is observed that the pressure drop increases at greater submergence ratios by 18% (from 2.95 to 3.60) (kg f/cm^2), due to friction and gravity; at the same time, making better use of the flow energy injected with the gas, unlike smaller submergences where the discharge presents higher pressures, wasting more flow energy. Meanwhile, the average Sgen decreases (from 0.342 to 0.296) KW/K as the submergence increases; which represents a greater use of flow energy for greater inmersions, for the experimental range of immersion ratios and gas injection areas at the nozzles.

The heat extracted in the geothermal flow increases (from 436 to 2694) (KW) thermal, when the immersion ratio is increased (from 0.80 to 0.91), while the average Sgen decreases (from 0.342 to 0.296) KW/K; this represents a greater use of the flow energy for the greater immersions. Therefore, less heat is lost from the lifting pipe of the l-g mixture towards the reservoir, which is colder. This is associated with an increase in the elevation velocity of the l-g mixture at greater immersion (from 0.23 to 1.05) m/s. This behavior can be observed in (Fig. 6).

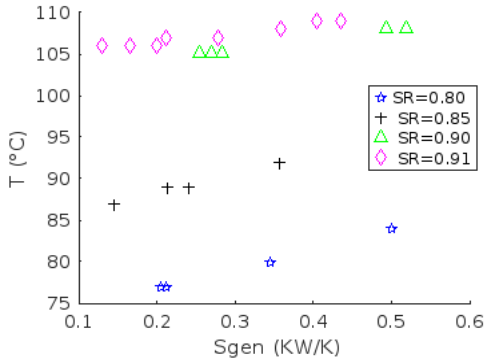


Fig. 3) The temperature of the extracted brine increases with the submergence ratios while the average Sgen decreases.

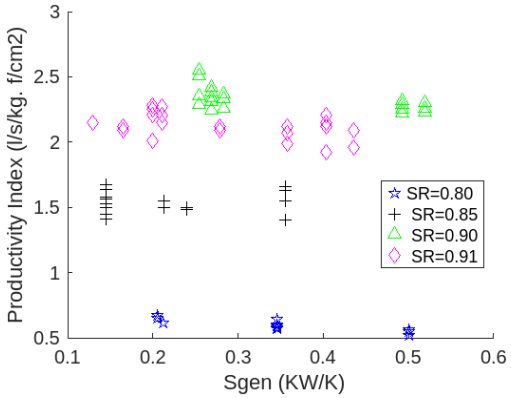


Fig. 4) The productivity index increases with submergence ratios while the average Sgen decreases.

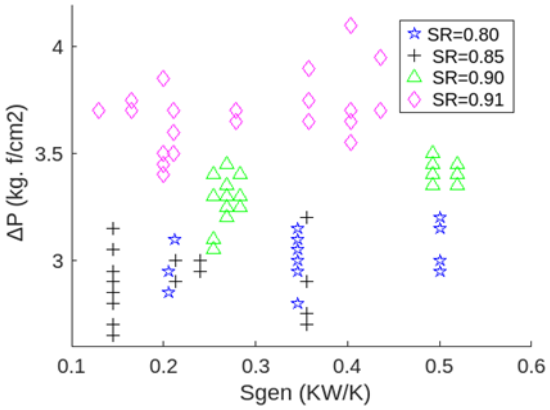


Fig. 5) The pressure drop increases with greater submergence ratios; while the average Sgen decreases with increasing immersion (from 0.80 to 0.91).

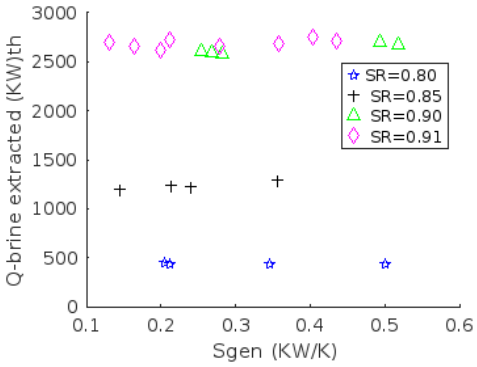


Fig. 6) Heat extraction increases with greater submergence ratios, making better use of the flow energy in the pipe, while the average Sgen decreases with increasing immersion (from 0.80 to 0.91).

2.8 Combined Uncertainty

The combined uncertainty of the experimentation is estimated using equation (2.12) (Smichd and Lazos, 2000). Where F is a dependent variable (or indirect measurements, such as Sgen) and Xn are the independent variables (direct measurements, such as pressure, temperature, and flow rate). The instruments used are: an orifice plate flow meter with an accuracy of ±2%; a variable area flow meter for air at the compressor outlet with an accuracy of ±2%, bimetallic thermometers with an accuracy of ±2%. The combined uncertainties of the variables estimated in (Table 3) are shown below.

$$U^2{}_F = \left(\frac{\partial F^2}{\partial X_1}\right)^2 UX_1^2 + \left(\frac{\partial F^2}{\partial X_2}\right)^2 UX_2^2 + \ldots + \left(\frac{\partial F^2}{\partial X_n}\right)^2 UX_n^2 \quad (2.12)$$

Table 3. Combined uncertainty rate UF for experimental data.

Variables	Uncertainty combined (U_F)	Error (%)
ΔProductivity Index (l/s/kg-f/cm2)	± 0.03	1.4
ΔQ_reservoir (KW)	± 12.52	1.68
ΔSgen (KW/K)	± 0.005	0.46

2.9 Conclusions

The airlift pumping system is used to extract geothermal brine from a 1,344-meter-deep well. Submergence rates are varied, and different large-area injectors are used, injecting a constant gas flow rate. The data obtained show that both the extracted brine flow rate (l/s) and temperature (°C) increased 78% and 40°C respectively when immersion is increased (from 0.80 to 0.91) and when larger gas injectors areas are used. The increase in the extracted brine flow rate at greater depths occurs because, with the increase in pressure drop, the flow energy injected with the gas is better utilized; unlike at smaller depths, which have a higher discharge pressure toward the surface, thus wasting flow energy. Additionally, the extracted flow increases, although to a lesser extent, when larger area injectors are used. On the other hand, the increase in temperature at greater immersions occurs because; with the increase in velocity of the mixture in the riser pipe, less heat is transferred to the reservoir, which is colder. The findings prove how average Sgen presents a decrease both with greater submergence ratios and larger area injectors which explains the increase in the temperature and flow rate, as confirmed by the works of (Hanafizadeh et al., 2011 and Julia et al., 2011) and (Pan et al., 2019 and Gutierrez et al., 2024). Furthermore, the increase in heat extraction from the geothermal brine is associated with a decrease in average Sgen and an increase in productivity, both for higher submergence ratios and larger injection areas, even though heat loss to the reservoir also increases, the heat rate (extracted/lost) increases each time under the aforementioned operating conditions. Therefore, in this study, Sgen and the productivity index are primarily influenced by the submergence ratios and the size of the injection areas; increasing both allows for increased heat extraction from the geothermal brine (within the experimental range), reducing the heat transfer rate from the riser pipe to the reservoir. Radial injection has better results than axial injection due to the larger injection

areas in the nozzles. Finally, we recommend continuing research into larger immersion ratios as well as injection areas in gas injectors using numerical simulation, and studying dual (axial-radial) and pulsating gas injection.

Acknowledgements

[sic] Coordinación de Investigación Científica, UMSNH.

Nicola Sattler and Barbara Thompson, my English teachers at YMCA, thank you for all your support.

3. REFERENCES

Ahmed, W. H., Aman, A. M., Badr, H. M., & Al-Qutub, A. M.: Air injection methods: The key to a better performance of airlift pumps, Experimental Thermal and Fluid Science, (2016), Volume 70, (2016), pages 354-365.

Arslan O. (2010).: Exergoeconomic evaluation of electricity generation by the medium temperature geothermal resources, using a Kalina cycle: Simav case study, International Journal of Thermal Sciences, Volume 49, Issue 9, (2010), Pages 1866-1873.

Baujard C., A. Genter, A., Dalmais, E., Maurer, V., Hehn, R. Rosillette, R., Vidal, J. Schmittbuhl, J.: Hydrothermal characterization of wells GRT-1 and GRT-2 in Rittershoffen, France: Implications on the understanding of natural flow Systems in the Rhine graben, Geothermic's, (2017), Volume 65, Pages 255-268.

Beasley, D.E & Liburdy, J.A.: Two phase flow characteristics of an airlift pump using small diameter tubes. Proceedings, International symposium on multi-phase transport and particulate phenomena; Miami Beach, FL USA (1986).

Bejan, A.: Convection Heat Transfer, John Wiley and Sons Inc., Fourth Edition, (2013), pages 31-34.

Cengel, Y. A., Boles M.A.: Termodinámica, McGraw-Hill Companies, 7th Edition México, (2011), pages 142, 189, 251, 351-356, 937.

De Cachard, F., & Delhaye, J. M.: A slugh-churn flow model for small-diameter airlift pumps, International Journal of Multiphase Flow, Volume 22, Issue 4, (1996), pages 627-649.

Davis A. P., and Michaelides E.E.: Geothermal power production from abandoned oil wells, Energy, Volume 34, Issue 7, (2009), pages 866-872.

Fan, W., Chen, J., Pan, Y., Huang, H., Chen, C. T. A., & Chen, Y.: Experimental study on the performance of an airlift pump for artificial upwelling, Ocean Engineering, Volume 59, (2013), Pages 47-57.

Favre-Marient, M. and Tardu, S.: Convective Heat Transfer, John-Wiley and Sons Inc, First Edition, (2009), pages 119-351.

Fisch, H., Uhde, J., Bems, C., Lang, P., Bartels, J.: Hydraulic testing and reservoir characterization of the Taufkirchen site in the Bavarian basin, Proceedings, World Geothermal Congress, Melbourne, Australia, (2015).

Smichd, W. and Lazos, R.: Guía para estimar la incertidumbre en la medición, Centro Nacional de Metrología (cenam), (2000), pp. 1-27.

Gutiérrez-Martínez, J; Pacheco, J. J; Aguilar-Corona, A; Figueroa-Espinoza, B.: Experimental study of an annular (concentric pipe) airlift system: effect of injection nozzle design. Journal of Fluid Fluids Engineering, ASME, Volume 146, Issue 12, (2024), 146(12): 121404 (11 pages).

Hanafizadeh, P., Ganbarzadeh, S., Hassan Saidi M.: Exergy analysis of airlift Systems: experimental approach, Int. J. Exergy, vol. 8, no.4, (2011), pages 407-424.

Hanafizadeh, P., Saidi, M. H., Darbandi, M., Kebriae, A.: Numerical simulation of two-phase flow in airlift pumps using the physical influence scheme, Progress in Computational Fluid Dynamics an International Journal, (2010) 10 (3), pages 186- 194.

Julia, J. E., & Hibiki, T.: Flow regime transition criteria for two-phase flow in a vertical annulus, International Journal of Heat and Fluid Flow, (2011), 32(5), pages 993-1004.

Krasniqi, D., Selimaj, R., and Krasniqi, M.: Thermal Dynamic Analysis of Parallel and Counter Flow Heat Exchangers, International Journal of Mechanical Engineering and Technology (IJMET), Volume 9, Issue 6, 2018, pp. 723–729.

Kumar, E.A., Kumar, K.R.V., Ramayya, A.V.: Augmentation of airlift pump performance with tapered upriser pipe- an experimental study, Journal of the Institution of Engineers (India): Mechanical Engineering Division 84(3):114-119.

Lund, J. and Toth, A.: Direct Heat Utilization of Geothermal Resources Worldwide Review. Proceedings, World Geothermal Congress, Reykjavik, Iceland, April 26 – May 2, (2020).

Ligus, G., Zając, D., Masiukiewicz, M., & Anweiler, S.: A new method of selecting the airlift pump optimum efficiency at low submergence ratios with the use of image analysis. Energies, 12(4), (2019), 735.

Margaris, D.P. and Papanikas, D.G.: A generalized gas-liquid-solid three-phase flow analysis for airlift pump design, Journal of Fluids Engineering, 119(4), (1997), 995-1002 (8 pages).

Nenes, A., Assimacopoulos, D., Markatos, N. and Mitsoulis, E.: Simulation of airlift pumps for deep water wells, Int. J. Multiphase Flow, 23 (7), (1997), 58.

Michaelides E.E.: Thermodymanic properties of geothermal fluids, Geothermal Resources Council, Transactions Volume 5, (1981), pp. 361-364.

Mitali, J., Dhinakaran, S., Mohamad A. A.: Energy storage systems: a review. Energy Storage and Saving, Volume 1, Issue 3, (2022), Pages 166-216.

Najeeb, S. (2017). Natural-Convection Phenomenon from a Finned Heated Vertical Tube: Experimental Analysis, Al-Khwarizmi Engineering Journal, Volume 13, No.4, (2017), pp 30-4.

Oueslati, A., & Megriche, A.: The effect of liquid temperature on the performance of an airlift pump. Energy Procedia, Volume 119, (2017), Pages 693-701.

Pan, Y., Li, Y., Fan, W., Zhang, D., Qiang, Y., Jiang, Z. P., & Chen, Y. (2019). A sea trial of airlift concept artificial upwelling in the East China Sea. Journal of Atmospheric and Oceanic Technology, 36(11), (2019), 2191-2204.

Reinemann, D. J., Parlange, J. Y., Timmons, M. B.: Theory of small-diameter airlift pumps. International Journal of Multiphase Flow, 16(1), (1990), 113-122.

Samaras, V.C., Margaris, D.P. (2005). Two-phase flow regime map for airlift pump vertical upward gas–liquid flow, Int. J. Multiphase Flow, Volume 31, Issue 6, (2005), Pages 757-766.

White, F. M., Fluid Mechanics, Fourth Edition, MC Graw Hill, New York, USA, (1999).

Ware L. A. (2020). Literature Review on Modeling of Density Diff view on Modeling of Density Difference Pumping Hence Strategy for Geothermal, West Virginia University, Graduate Theses, Dissertations, and Problem Reports. (2020).

Zenz, F.A. (1993). Explore the potential of airlift pumps and multiphase systems, Chem. Eng. Prog., 89, (8), (1993), 51 (19).

Zuo, J., Li, F., Zhang, N., He, D., Wang, W., & Zhang, J. (2020). Experimental study on hydraulic characteristics of pneumatic lifting pump. Water, 12(2), (2020), 388.